CMUT for ultrafast passive cavitation detection during ultrasound-induced blood-brain barrier disruption: proof of concept study

Corentin Cornu, Laurène Jourdain, Flavien Barcella, Laurent Colin, Zoé Edon, Ambre Dauba, Erwan Selingue, Jean-Luc Gennisson, Benoit Larrat, Dominique Certon, et al.

CMUT for ultrafast passive cavitation detection during ultrasound-induced blood-brain barrier disruption: proof of concept study

Corentin Cornu[1,2], Laurène Jourdain[1], Flavien Barcella[3], Laurent Colin[3], Zoé Edon[1], Ambre Dauba[1], Erwan Selingue[2], Jean-Luc Gennisson[1], Benoit Larrat[2], Dominique Certon[3], Anthony Novell[1].

[1]Université Paris-Saclay, CEA, CNRS, Inserm, BioMaps, SHFJ, Orsay, France
[2]Université Paris-Saclay, CEA, Baobab, Neurospin, Saclay, France
[3]GREMAN UMR CNRS 7347, Université François Rabelais, INSA Centre Val de Loire, Tours, France

Corresponding author: anthony.novell@universite-paris-saclay.fr

Abstract

Objective. Cavitation dose monitoring plays a key role in ultrasound drug delivery to the brain. The use of CMUT technology has a great potential for passive cavitation detection (PCD).
Approach. Here, a circular (diameter 7mm) capacitive micromachined ultrasonic transducer (CMUT) centered at 5MHz was designed to be inserted into a therapeutic transducer (1.5MHz) used for ultrasound-induced blood-brain barrier (BBB) disruption on mice. CMUT-based real-time cavitation detection was performed during the ultrasound procedure (50µL intravenous injection of SonoVue microbubbles, Frequency 1.5MHz, PNP 480kPa, Duty Cycle 10%, PRF 10Hz, Duration 60s). BBB disruption were confirmed by contrast-enhanced 7T-MRI.
Main results. The CMUT device has a fractional bandwidth of 140%, almost twice a conventional piezocomposite PCD transducer. As expected, the CMUT device was able to detect the occurrence of harmonic, subharmonic and ultraharmonic frequencies as well as the increase of broadband signal indicating inertial cavitation in a wide frequency range (from 0.75 to 6 MHz). Signal-to-noise ratio was high enough (> 40 dB) to perform ultrafast monitoring and follow the subtle intrapulse variations of frequency components at a rate of 10 kHz.
Significance. This first *in vivo* proof of concept demonstrates the interest of CMUT for PCD and encourages us to develop devices for PCD in larger animals by integrating an amplifier directly to the CMUT front-end to considerably increase the signal-to-noise ratio.

Keywords

Focused ultrasound, CMUT, passive cavitation detection, microbubble, blood-brain barrier

1. Introduction

The primary challenge in delivering drugs and xenobiotics to the brain lies in the selective permeability of the blood-brain barrier (BBB) which regulates cerebral homeostasis. This barrier restricts access of large molecules to specific targets for treatment against neurodegenerative diseases, brain tumors and psychiatric illness. Focused ultrasound (FUS) combined with the injection of microbubbles has shown to enhance BBB permeability by inducing transcytosis and drug extravasation (1). At low acoustic pressures, ultrasound induces stable cavitation resulting in an alternation of expansion and shrinkage (push-pull mechanism) of microbubbles and microstreaming near the endothelial barrier, which contributes directly to tight junction disruption. Emission of harmonic components are associated with stable cavitation and can be exploited as indicators of efficient and safe BBB disruption. Conversely, high-intensity ultrasound exposure can trigger inertial cavitation, characterized by violent collapse, fragmentation of microbubbles, micro-jets, and shock waves, resulting in broadband emissions. The presence and significance of subharmonic and ultra-harmonic frequency components as indicators of harmful microbubble activity are still a subject of debate (2). However, it is generally accepted that the inertial cavitation regime should be avoided as it may cause undesirable vessel damage. Without proper parameters and precise control of the ultrasound dose, the collapse of microbubbles can lead to undesirable bioeffects such as neuroinflammation, edema, and hemorrhage (3-5). Maintaining a constant and efficient cavitation level during the procedure remains challenging as the dynamic behavior and the concentration of microbubbles vary over time. Acoustic monitoring of the non-linear backscattered response based on cavitation detection is currently the only way to control in real-time the ultrasound dose during sonication and ensure effective and safe disruption of the BBB (6, 7).

Ultrasound propagation through the skull is a major challenge in FUS-induced BBB opening. For PCD, the skull attenuates and filters the backscattered signal from microbubbles making its processing difficult. Especially when considering applications to large animal or human brains, the heterogeneity of the skull leads to great disparity depending on the position of the ultrasound beam, inducing high attenuation and scattering characterized by focus aberration, presence of stationary waves, reflections and attenuation of the signal (8, 9).

Recently, we demonstrated that ultrafast cavitation monitoring can be performed to distinguish potentially harmful to safe ultrasound conditions in the brain with very short reaction time (2). Briefly, this new indicator is based on the detection of sudden variation in ultraharmonic activity inside an ultrasound burst. Using this approach, it would be possible to prevent any damages into brain by controlling the ultrasound dose in less than 100 µs. Its implementation is based on the spectral analysis of relatively short temporal windows and requires high-sensitivity signal detection.

The sensitivity of transducers used for passive cavitation detection (PCD) is hampered by the limited bandwidth of standard transducers. This limitation makes it difficult to capture a wide range of frequencies at high sensitivity, as skull-induced attenuation further reduces signal amplitude, acting as a low-pass filter. The most commonly used PCD technologies are ferroelectrics, such as lead zirconate titanate (PZT) (10), and polymers like polyvinylidene fluoride (PVDF) (11). PZT-based PCDs offer good sensitivity but have a relatively narrow bandwidth (about 60-80%). Although more complex to manufacture, piezocomposite

materials provide a higher electromechanical coupling coefficient than basic PZT ceramics, resulting in an improved signal-to-noise ratio and better signal detection but their bandwidth remains limited. On the other hand, some studies use PVDF-based broadband hydrophones, which have a wide bandwidth but suffer from a lack of sensitivity. In this context, Capacitive Micromachined Ultrasonic Transducers (CMUTs) exhibit interesting properties for PCD (12, 13). Capacitive sensors operate on the principle of an ideal plate capacitor. Each CMUT element is made up of several hundreds of elementary cells acting as a set of interconnected capacitors in which flexible plates (made typically of silicon or silicon-nitride) are positioned between two electrodes. When an electrical signal is transmitted to the sensor, the modulation of the electrostatic force between the two electrodes induces a vibration of the plate, resulting in the generation of an acoustic wave. Conversely, when a mechanical wave is applied to the plate, the resulting vibration causes a variation in the cell's intrinsic capacitance, and hence a receiving current that can be measured (14). The operating principle of a CMUT is illustrated in Figure 1. Polarization of the CMUT (addition of a biasing voltage) is necessary to facilitate plate movement and thus increase sensor sensitivity. CMUT technology offers advantages such as wide bandwidth. Used in receive mode, CMUTs may detect non-linear components usually not observable with PZT, while offering better sensitivity than PVDF hydrophones (13). In addition, dedicated amplifiers can be integrated directly into CMUT circuit boards to improve sensitivity in receive mode. The main drawback of CMUT lies in its intrinsic non-linear behavior, which can mask the acoustic emissions of microbubbles (15). However, this non-linearity can be controlled to be as low as acceptable (fundamental-to-harmonic ratio > 30 dB) by modulating the applied biasing voltage (16). This study aims to validate the first use of a CMUT-based PCD for ultrafast cavitation monitoring during BBB opening *in vivo*.

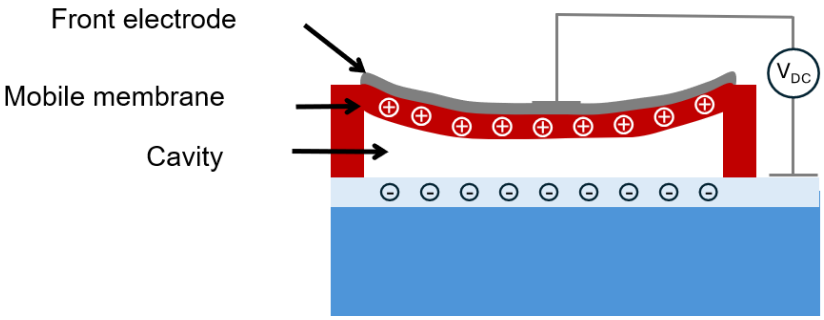

Figure 1. Diagram of a CMUT illustrating its operating principle. When an ultrasonic wave impinges the mobile front electrode of the CMUT, it produces variations in electrical charges, which create the receiving electrical signal.

2. Material and Methods

2.1 CMUT Design

The transducer (Figure 2) was designed to meet specifications from the applications, i.e. a small footprint (final housing diameter of 3.7 mm) and a central frequency close to 4 MHz with a frequency bandwidth higher than 100 %. A sketch of the transducer is shown in Figure 2a. The chip was a square of 2.6 mm width, and the CMUT transducer diameter was fixed to have a diameter of 2.6 mm. A surface micromachining process was used for CMUT fabrication (17). The structural and electrode material of the CMUT plate were silicon nitride and aluminum, respectively (Table 1). The gap thickness was determined to get a collapse voltage value lower

than 100 V. CMUT aligned horizontally are electrically connected to the same electrode, and the CMUT-to-CMUT kerf was fixed to a minimum value of 8 µm. The kerf along the vertical direction was fixed to 12 µm. Finally, the membrane size (32x32 μm^2) was determined by using the model from Meynier *et al.* (18) to comply with specifications. Table 2 summarizes all the CMUT parameters, and the collapse and resonance frequency (in air) expected. The CMUT was packaged in a specific housing as shown in Figure 2b, and then covered with a biocompatible silicon polymer of 300 µm thick.

Table I. Mechanical and dielectric properties of materials

	Dielectric constant	Young's modulus (GPa)	Density ($kg.m^{-3}$)	Poisson's ratio	T_0 (MPa)
Aluminum		68	2700	0.35	0
Silicon Nitride	7.5	230	3300	0.24	270

Table II. CMUT cell characteristics

CMUT size	32 µm x 32 µm
Membrane thickness	450 nm
Gap height (measured)	270 nm
Top electrode size	32 µm x 32 µm
Top electrode thickness	450 nm
Collapse voltage	89 V (theory) – 85 V (measured)
Resonance frequency in air	8.2 MHz (theory) – 8 MHz (measured)

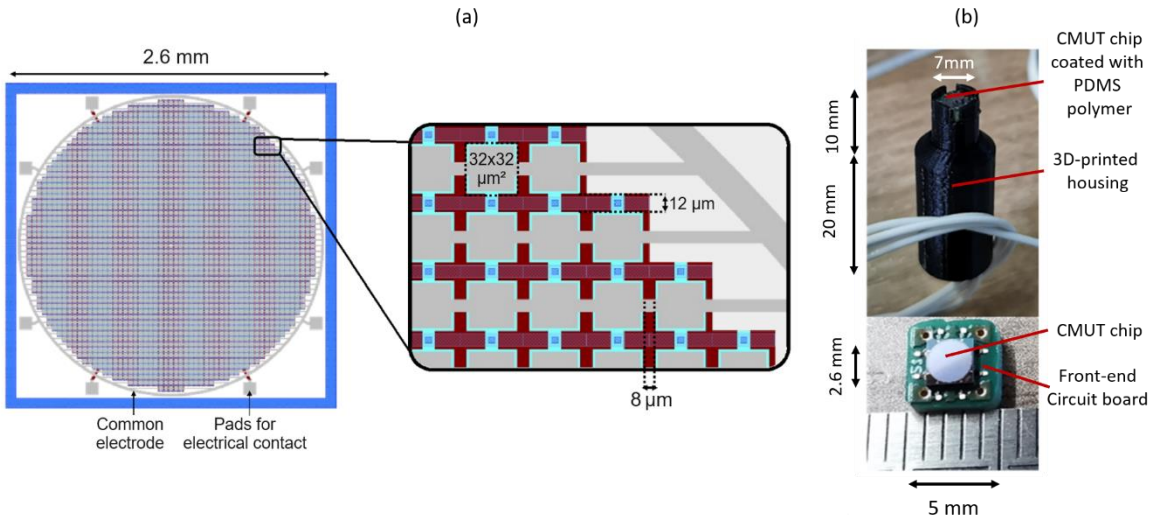

Figure 2. (a) Sketch of the CMUT chip: representation of the transducer and CMUT layout. (b) Picture of the CMUT-based PCD showing the transducer housing (Top) and a zoom on the integrated front-end circuit board connected to the CMUT element (Bottom). A PDMS silicone polymer is used as coating to protect the chip.

2.2 CMUT fabrication tests and acoustical measurements

Multiple characterizations were performed to assess the transducer performances. First, electrical impedance was measured with 4294A Impedance Analyzer from (Keysight, CA, USA), from which the low frequency capacitance (C_{BF}) measured at 100 kHz was extracted. The

biasing voltage was increased from 0 to 100 V with a pitch of 10 V, and then, decreased to 0 V.

Then, the impulse response of the CMUT transducer was determined by using a “pitch-catch”measurement between two similar transducers, fabricated from the same wafer. A pulser was used (model 5077 PR from Olympus Company, Japan), and the electrical excitation bandwidth was fixed to 10 MHz with amplitude of 15 Volt. A distance of 45 mm and a gain in receive of +20 dB were chosen.

Finally, sensitivity of the CMUT-based PCD was measured in receive mode by using an acoustic pressure source (PVDF transducer, model PA2244, diameter of 27 mm, Precision Acoustics, UK) calibrated by a hydrophone (model NH4000, Precision Acoustics) placed in the near field area of the transducer. The distance was chosen at 20 mm to correspond to the focal distance of the therapeutic transducer used for *in vivo* experiments. Excitation signal (30 V_{pp}) was a burst of 3 periods with a varying frequency from 0.5 to 10 MHz with a step of 0.2 MHz. The sensitivity of the CMUT in receive was obtained by measuring the peak-to-peak amplitude of the signal divided then by the peak-to-peak incident pressure amplitude. The signal was amplified by 20 dB using the 5077 PR.

2.3 *In vivo* protocol

In vivo experiments were performed on mice (n=4, C57BL/6, 17-24 g, Janvier, France). The experimental protocol was approved by a local ethics committee for animal use (CETEA) and by the French ministry of agriculture authorization APAFIS#16293-2018072609593031/ethics committee number 44. The mice were anesthetized with isoflurane (1-1.5%) in a mixture of air and oxygen.

A circular ultrasonic transducer (center frequency: 1.5 MHz, diameter: 20 mm, focal depth 20 mm; Imasonic, France) was designed with spherical shape and a hole (7 mm) in the center for the placement of the CMUT-based PCD (Figure 3a). The animal's head was shaved, and the ultrasound transducer was coupled to the head via a water balloon and ultrasound gel. A bias voltage (model 9185, B&K Precision, Taiwan) corresponding to 80% of the collapse voltage was applied to the CMUT-PCD to increase its sensitivity while preserving an acceptable intrinsic nonlinear level.

First, a baseline sequence at gradually increasing pressure was acquired prior to the injection of microbubbles to check the ultrasound coupling and define cavitation thresholds. Then, microbubbles (dose: 2 mL/kg; SonoVue, Bracco Imaging, Italy) and gadolinium MRI contrast agent (4 mL/kg; Dotarem, Guerbet, France) were administered in the tail vein. A single spot sonication (sinusoidal burst at 1.5 MHz, peak negative pressure in situ 0.45MPa, pulse repetition frequency 10 Hz, pulse length 9 ms) was applied at a single point for 1 min. The transducer was driven by an ultrasound generator (CUBE, Image Guided Therapy, France). To avoid overshoots and transient behaviors, the amplitude gradually increased until reaching the target pressure (during 650 µs) at the beginning of the pulse and gradually decreased at the end of the pulse.

MRI T1w images were acquired 5 min after US exposure to validate BBB disruption after MR contrast agent administration (Figure 3b). MRI acquisitions (TR: 300ms, TE: 8ms, 8 averages, 128/128 resolution, 14 coronal slices, slice thickness 0.6mm) were performed in a 7-T preclinical scanner (Pharmascan, Bruker, Germany).

2.4 Ultrafast cavitation detection

The signal detected by the CMUT was amplified (20 dB, Pulser/Receiver DPR300, JSR Ultrasonics, France), and acquired by the Digital to-Analog Converter of an FPGA module (Field-Programmable Gate Array, NI PXIe-7971R board, Austin, TX, 16-bit, 25 MHz sampling frequency, NI-5783 module, USA). The FPGA process was controlled by a software developed in Python and raw acoustic signals were saved on the host computer (Figure 3c). Briefly, for real-time analysis, these data were sliced into successive Hann windows on the pulse (2048 values corresponding to 82 µs) that overlapped every 41 µs. A Fast Fourier Transform was then applied on each window. As displayed in Figure 3d, cavitation indexes based on

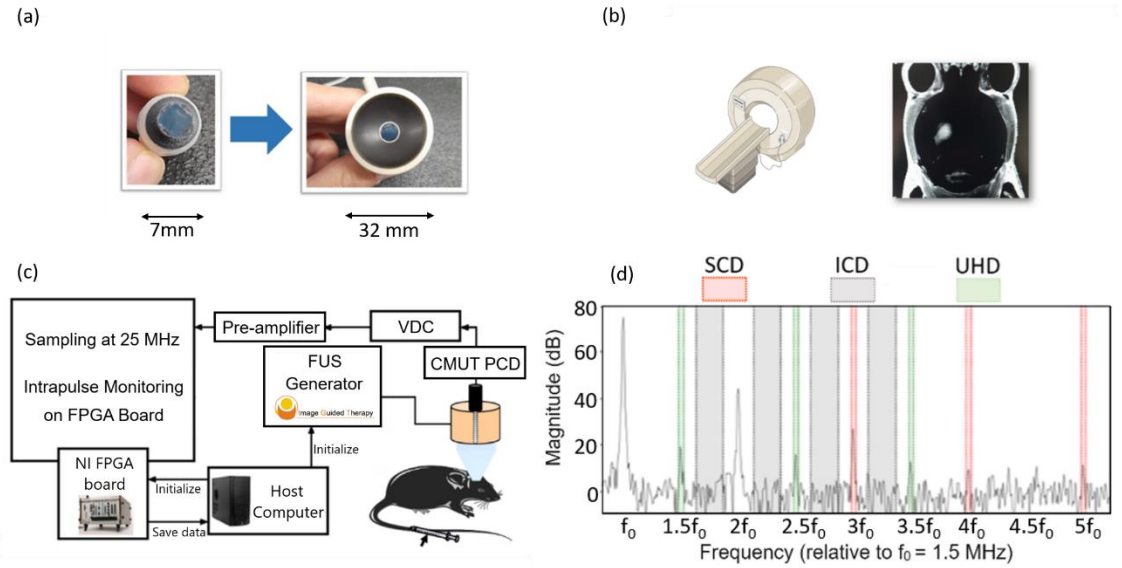

Figure 3. (a) Picture of the CMUT-based PCD inserted into the therapeutic transducer. (b) 7T-MRI of a mouse brain after FUS-induced BBB disruption. (c) Scheme of the ultrafast PCD. (d) Example of a spectral response of microbubble cavitation. Frequency bands considered for the dose calculation (gray: inertial; red: stable; green: sub and ultra-harmonics).

ultraharmonics (UHD at $1.5f_0$, $2.5f_0$ and $3.5f_0$) and harmonics (SCD at $3f_0$, $4f_0$ and $5f_0$) contents were determined by calculating the area under curve around the considered frequency component *f*, as described by the formula:

$$AUC(f) = \frac{1}{N(k)} \sum_{k=\mathrm{kmin}}^{\mathrm{kmax}} |\mathrm{P[k]}|$$

with |P[k]| the magnitude of the discrete Fourier transform, *N(k)* the number of points in the considered frequency band, and kmin and kmax the minimum and maximum indices corresponding to the discrete frequency range of interest (band of 61 kHz) for each harmonic and ultraharmonic components. The $2f_0$ component was excluded from the calculation because the signal was polluted by nonlinear reflection. The inertial cavitation dose (ICD) was calculated as the area under the broadband spectral noise curve over four 195 kHz-wide frequency bands chosen between harmonic and ultraharmonics peaks (see Figure 3d). Each of the SCD, UHD and ICD indices were normalized by the area under curve of a reference window (AUC_{ref}) corresponding to the electronic noise. This reference window is acquired on 328 µs, just before emission of the ultrasound pulse. SCD, UHD and ICD were then converted in dB. Finally, all indices were smoothed with a moving average over 4 consecutive windows.

3. Results

3.1 CMUT performances

Figure 4a shows C_{BF} variations according to the biasing voltage. A collapse voltage (corresponding to drop in the capacitance variations) close to 85 V was measured while 89 V was expected based on our model (Table 2). The biasing voltage for using CMUT was fixed, for all experiments to 70V, i.e. 80% Vc to optimize the tradeoff between sensitivity versus non-linearity (for a biasing voltage of 70V, the harmonic to fundamental ratio was measured at -36dB, data not shown).

The impulse response is shown in Figure 4b. The corresponding spectrum shows a central frequency of 3.8MHz and a -6dB fractional bandwidth of almost 140% (from 1.2MHz to 6.5MHz) as displayed in Figure 4c.

The sensitivity (in dBV/MPa) of the CMUT device in receive mode is shown in Figure 4d. The maximum sensitivity was reached at 2 MHz (5.5 V/MPa) and then decreases slowly for higher frequency. The shape of the reception sensitivity curve strongly depends on the type of preamplifier circuit used, voltage or transimpedance(19).

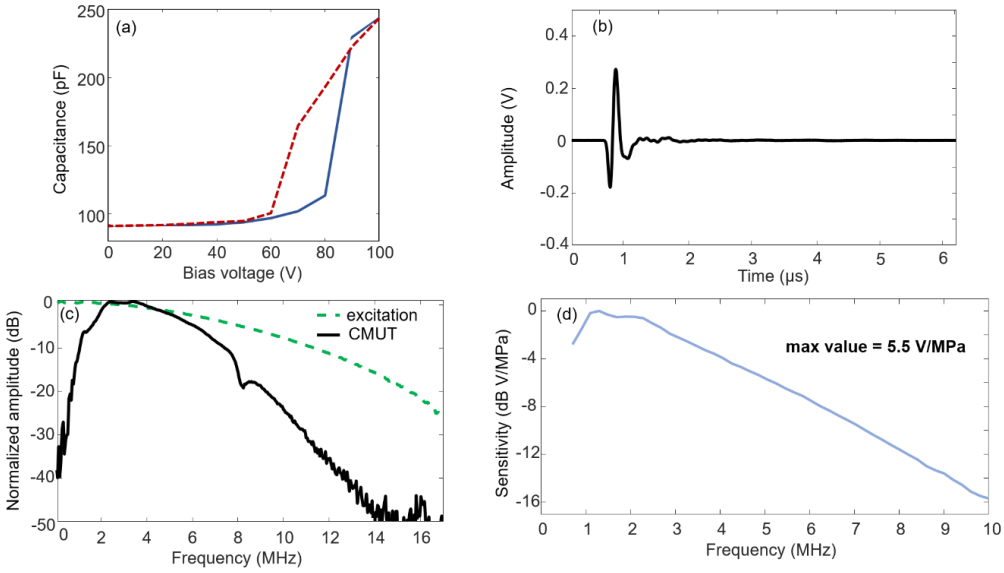

Figure 4. Characterization of the CMUT. (a) Low frequency capacitance of the CMUT transducer, measured at 100 kHz, according to the biasing voltage (solid line in blue from 0V to 100 V, dashed line in red from 100 V to 0V). (b) Impulse response of the transducer. (c) Frequency response, dashed line corresponds to the excitation spectrum. (d) Experimental reception sensitivity of the CMUT transducer. The maximum sensitivity is 5.5 V/MPa.

3.2. *In vivo* ultrafast cavitation detection

Figure 5a shows an example of a spectrogram obtained with conventional pulse-to-pulse analysis. The figure shows the evolution of the spectral response over the 600 pulses making up the ultrasonic sequence, repeated every 10Hz for 1 min. In this figure, only the fundamental component at f_0 and the harmonics at $2f_0$ and $3f_0$, as well as a weak $4f_0$, are visible. The benefits of intrapulse detection and the sensitivity of the CMUT sensor are demonstrated in Figure 5b.

This curve shows the evolution of UHD and ICD indexes by conventional (black) and intrapulse (gray) analysis during the FUS sequence. It is clear that intrapulse analysis enables a far greater number of events to be detected. Figures 6a and 6d show examples of spectrograms of backscattered signals captured for pulses located at the beginning of FUS exposure (Pulse #21) and at the end of FUS exposure (Pulse #407), respectively. Contrary to conventional analysis (Figure 5a), these spectrograms show the evolution of frequency content within a single 10 ms pulse of the FUS sequence. First, intrapulse sliding-window analysis enables the detection of ultraharmonic ($2.5f_0$ and $3.5f_0$) and broadband (mainly from $0.5f_0$ to $2f_0$) content unobservable with conventional analysis. In fact, the events detected are transient and generally last only a few hundred of µs, making them extremely difficult to observe with whole-pulse analysis. Secondly, intrapulse analysis reveals 2 types of ultraharmonic signatures: either they appear suddenly during the pulse and are maintained until the end of the pulse (Figure 6a), or they occur right from the start and disappear within a few µs (Figure 6d). In the latter case, these ultraharmonic events are often associated with the detection of broadband noise. Interestingly, CMUT technology is sensitive enough to detect these brief and weak events and extract the signal from the noise. Examples of frequency spectra calculated during intrapulse analysis at different time windows are given in Figure 6 (b-c, e-f). The sudden appearance of the ultraharmonic at 1.5 f_0 in the spectral content can be easily observed by comparing the spectra obtained for the same pulse (#21) at different time windows (b-c). Conversely, the sudden disappearance of the ultraharmonic component at 1.5 f_0 can be seen in the spectral representations of pulse #407 at different time windows (e-f). Furthermore, one can note the presence of substantial broadband noise in spectrum (e), which diminishes over time (f).

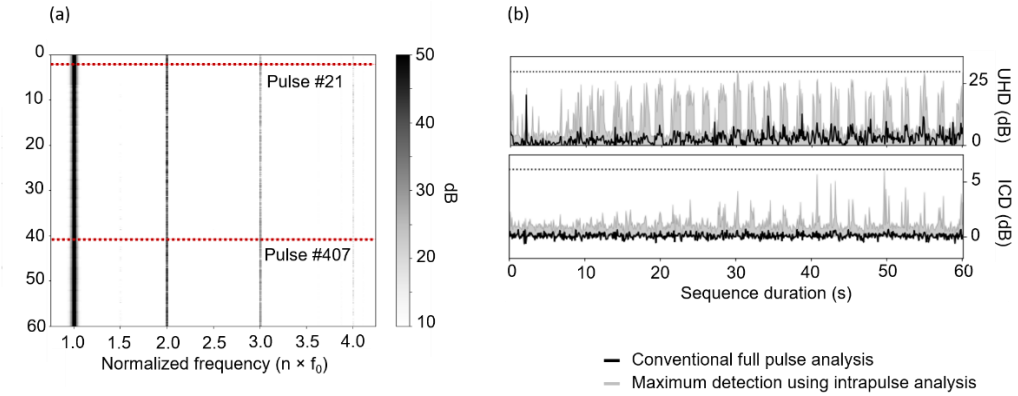

Figure 5. (a) Spectrogram calculated from conventional analysis of data acquired by CMUT-based PCD during FUS sequence. (b) PCD analysis for UHD and ICD using conventional and intrapulse methods.

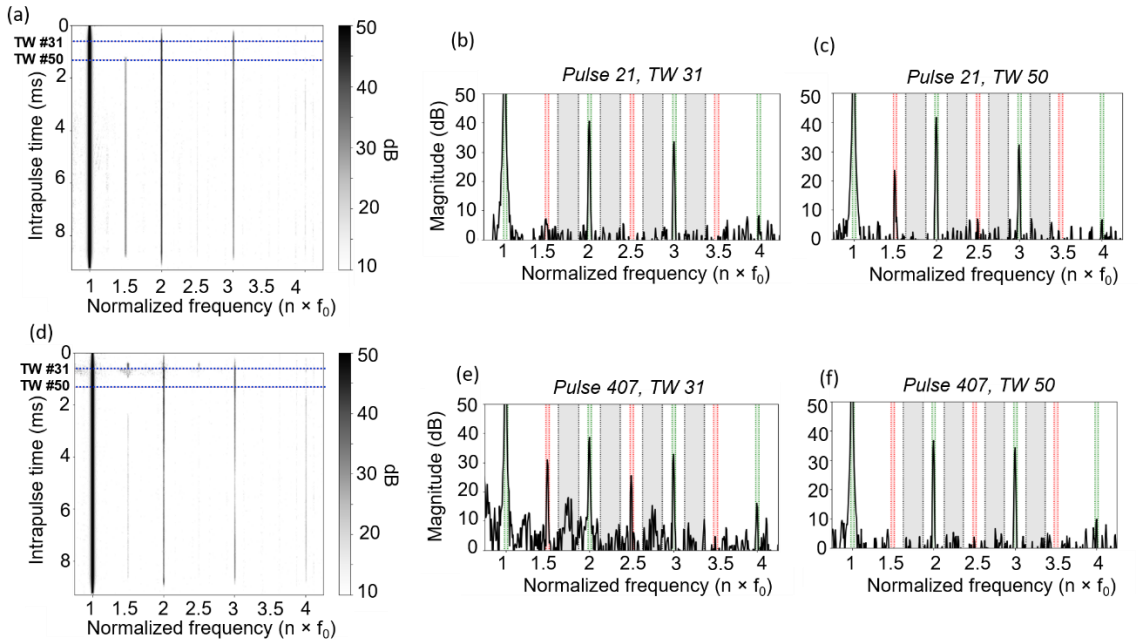

Figure 6. Examples of spectrograms calculated from intrapulse analysis acquired (a) at the beginning of ultrasound exposure (Pulse #21) and at the end of ultrasound exposure (Pulse #407). Examples of frequency spectra calculated during intrapulse analysis at different time windows (TW) are given in panels (b-c, e-f).

For harmonic components and SCD calculations, $2f_0$, $3f_0$, and $4f_0$ show the same sensitivity (about +14 dB compared to baseline), as shown in Table III. As expected, the $2f_0$ component is heavily polluted by nonlinear propagation of the ultrasound wave through the skull and multiple signal reflections at interfaces. The intrinsic nonlinearity of the CMUT also interferes with this measurement, adding an undesirable harmonic signal. For ultraharmonic components and UHD calculation, the $1.5f_0$ component (+22 dB vs. baseline) is far more sensitive than the others. Even without a dedicated amplifier, the bubble signal is detectable down to $4f_0$. The bandwidth of our CMUT sensor means that the contributions of these different components can be added together to calculate cavitation indices, thereby increasing the sensitivity of our detection method.

Table III. Typical dynamic range of AUC (dB) for harmonics, ultraharmonics and broadband signal measured with the CMUT device.

Frequency component	$1.5f_0$	$2f_0$	$2.5f_0$	$3f_0$	$3.5f_0$	$4f_0$	Broadband
Baseline (no bubbles)	7.29	32.20	5.63	8.07	5.67	8.07	1.31
FUS sequence (BBB opening)	29.69	46.64	22.53	36.44	11.39	22.13	6.23

Figure 7a presents the comparison between the UHD (including $1.5f_0$, $2.5f_0$, $3.5f_0$) and the ICD index. The scatter plots consist of two overlapping sets: (1) the baseline shot, prior microbubble injection, depicted in grey, and (2) the indexes during the FUS-induced BBB disruption, illustrated in black. Results effectively discriminate between the presence and absence of microbubbles. The black lines represent the threshold values used to differentiate

cavitation states. The figure demonstrates a prominent UHD cavitation regime with a limited number of inertial cavitation events. In Figure 7b, the appearance of both inertial and ultraharmonic events inside a pulse is illustrated. Using our FUS parameters, ultraharmonic events exhibit a greater prevalence compared to inertial events. While most ICD events exclusively occur at the beginning of the pulse, UH events are also observable later in the pulse (between 1ms and 5ms). The two modes (named "transient" and "sustained") are differentiated according to the duration of the detected event (< or > 1 ms). The average duration of transient and sustained events is 0.50 ± 0.21 ms and 4.16 ± 2.80 ms, respectively.

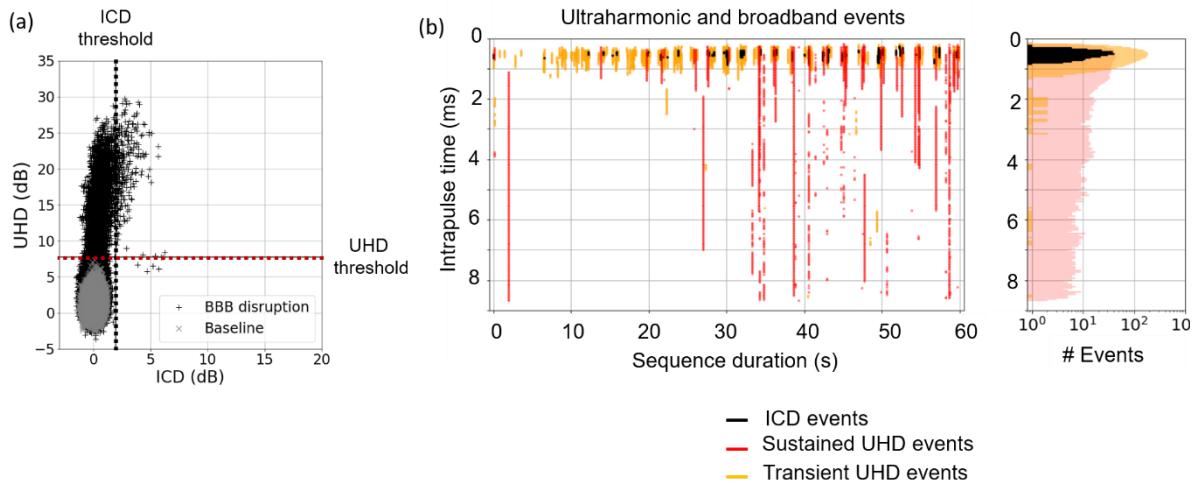

Figure 7. (a) Representation of the intrapulse ultraharmonic dose (UHD) and the intrapulse inertial cavitation dose (ICD) during the FUS sequence. (b) Intrapulse detection of ultraharmonic and broadband events during the FUS sequence. UHD events are separate between transient and sustained.

4. Discussion and conclusion

The efficient monitoring of cavitation activity has been confirmed using CMUT PCD having a wider bandwidth compared to traditional PZT transducers. To detect intrapulse events, the spectral analysis was performed on narrow temporal windows of approximately 80 µs. Processing the data analysis on short temporal windows significantly reduces the signal to noise ratio and makes the detection of nonlinear content challenging. CMUT PCD has shown promising results, demonstrating its ability to effectively detect inertial cavitation events and very brief variations on ultraharmonic content with a high sensitivity.

Most existing control strategies for real-time cavitation monitoring employ a pulse-to-pulse approach, where decisions regarding modulating the ultrasound beam amplitude (5, 20-22) and/or ending sonication once the threshold is reached (23-26) are made based on cavitation doses processed over the entire pulse. Our results reveal two important findings. Firstly, punctual cavitation events (UHD and ICD, shown in Figure 6d) occur at the beginning of the pulse. The next step will be to correlate the detection of these brief UHD and ICD events with the effects observed (presence of edema, petechiae) to define the threshold of dangerousness of these signatures and design a feedback control algorithm. Novell *et al.* (2) have proposed the hypothesis that ultraharmonic events occurring later in the pulse (after 1ms) could be associated with destabilization preceding stronger inertial cavitation events, which are linked to edema and hemorrhages. Our intrapulse monitoring (Figure 7b) does show the presence of

some of these events. A control strategy based on real-time monitoring combined with the advantageous bandwidth of CMUT-based PCD could enhance the detection of the destabilization regime of microbubbles through the skull. Thus, the ultrafast FPGA measurement developed in our study (every 80 µs) can be used to detect the acoustic signature of undesirable events as quickly as possible and then adjust inside the pulse the acoustic pressure emitted. In this respect, FPGA-assisted control strategies applied *in vitro* (27, 28) have already demonstrated that it is possible to implement feedback loop control within pulses. Secondly, notable differences are observed between doses processed using the entire pulse signal and those based on maximum instantaneous values, particularly for ultraharmonics as shown in Figures 5 and 6. Therefore, processing cavitation dose over the entire pulse duration may conceal brief yet intense bursts of cavitation.

Finally, the presence of the fundamental component f_0 and harmonic $2f_0$ does not provide any specific information regarding bubble-induced non-linearities due to the nonlinear propagation and the reflection induced by the presence of the skull. The nonlinearity of the CMUT will also pollute the signal from $2f_0$, even in receive mode. Therefore, harmonics at $3f_0$ and above must be considered for the calculation of stable cavitation index, hence the interest to consider a larger broadband than conventional PCD. To increase even more the measured dynamics, techniques such as pulse inversion(29, 30) and phase keying strategies (31) are employed to strongly reduce the fundamental component. To apply these techniques with a high-quality input quantification dynamic (such as 16 bits in our system) could fully unleash the potential of CMUT-based PCD by effectively exploiting its bandwidth. Moreover, by integrating a pre-amplifier directly into the CMUT device, we anticipate a significant improvement in the signal-to-noise ratio. Very recently, Zangabad *et al.* has designed a new electronic device composed of a 16-channel analog front-end electronics with a low-noise transimpedance amplifier, a band-gap reference circuit, and an output buffer stage, that connected to a commercial CMUT array for passive cavitation detection. This has been validated *in vitro* for the detection of microbubble acoustic emission (32). This huge advantage compared to conventional PZT technology will help to overcome challenges encountered with thicker skulls, particularly in large animals and for clinical applications.

Acknowledgements

This work was partly funded by ANR DROPMUT (grant ANR-19-CE19-0011), France Life Imaging (grant ANR-11-INBS-0006) and Inserm Plan Cancer (PCSI IMPETUS).

The authors would like to acknowledge Nicolas Sénégond (Vermon) for technical assistance.

Disclosure of competing interests

BL and AN are cofounders and stockholders of the company TheraSonic developing an ultrasound device for blood-brain barrier opening.

Data availability statement

The data cannot be made publicly available upon publication because they contain commercially sensitive information. The data that support the findings of this study are available upon reasonable request from the authors.

References

1. Hynynen K, McDannold N, Vykhodtseva N, Jolesz FA. Noninvasive MR imaging-guided focal opening of the blood-brain barrier in rabbits. Radiology. 2001;220(3):640-6.
2. Novell A, Kamimura HAS, Cafarelli A, Gerstenmayer M, Flament J, Valette J, et al. A new safety index based on intrapulse monitoring of ultra-harmonic cavitation during ultrasound-induced blood-brain barrier opening procedures. Sci Rep. 2020;10(1):10088.
3. Tung YS, Vlachos F, Choi JJ, Deffieux T, Selert K, Konofagou EE. In vivo transcranial cavitation threshold detection during ultrasound-induced blood-brain barrier opening in mice. Phys Med Biol. 2010;55(20):6141-55.
4. McDannold N, Vykhodtseva N, Hynynen K. Targeted disruption of the blood-brain barrier with focused ultrasound: association with cavitation activity. Phys Med Biol. 2006;51(4):793-807.
5. Arvanitis CD, Livingstone MS, McDannold N. Combined ultrasound and MR imaging to guide focused ultrasound therapies in the brain. Phys Med Biol. 2013;58(14):4749-61.
6. Arvanitis CD, Livingstone MS, Vykhodtseva N, McDannold N. Controlled ultrasound-induced blood-brain barrier disruption using passive acoustic emissions monitoring. PLoS One. 2012;7(9):e45783.
7. Sun T, Samiotaki G, Wang S, Acosta C, Chen CC, Konofagou EE. Acoustic cavitation-based monitoring of the reversibility and permeability of ultrasound-induced blood-brain barrier opening. Phys Med Biol. 2015;60(23):9079-94.
8. Pinton G, Aubry JF, Bossy E, Muller M, Pernot M, Tanter M. Attenuation, scattering, and absorption of ultrasound in the skull bone. Med Phys. 2012;39(1):299-307.
9. Pichardo S, Sin VW, Hynynen K. Multi-frequency characterization of the speed of sound and attenuation coefficient for longitudinal transmission of freshly excised human skulls. Phys Med Biol. 2011;56(1):219-50.
10. Deng L, O'Reilly MA, Jones RM, An R, Hynynen K. A multi-frequency sparse hemispherical ultrasound phased array for microbubble-mediated transcranial therapy and simultaneous cavitation mapping. Phys Med Biol. 2016;61(24):8476-501.
11. O'Reilly MA, Hynynen K. A PVDF receiver for ultrasound monitoring of transcranial focused ultrasound therapy. IEEE Trans Biomed Eng. 2010;57(9):2286-94.
12. Schoen S, Jr., Kilinc MS, Lee H, Guo Y, Degertekin FL, Woodworth GF, et al. Towards controlled drug delivery in brain tumors with microbubble-enhanced focused ultrasound. Adv Drug Deliv Rev. 2022;180:114043.
13. Dauba A, Goulas J, Colin L, Jourdain L, Larrat B, Gennisson JL, et al. Evaluation of capacitive micromachined ultrasonic transducers for passive monitoring of microbubble-assisted ultrasound therapies. J Acoust Soc Am. 2020;148(4):2248.
14. Khuri-Yakub BT, Oralkan O. Capacitive micromachined ultrasonic transducers for medical imaging and therapy. J Micromech Microeng. 2011;21(5):54004-14.
15. Novell A, Legros M, Felix N, Bouakaz A. Exploitation of capacitive micromachined transducers for nonlinear ultrasound imaging. IEEE Trans Ultrason Ferroelectr Freq Control. 2009;56(12):2733-43.
16. Novell A, Legros M, Gregoire JM, Dayton PA, Bouakaz A. Evaluation of bias voltage modulation sequence for nonlinear contrast agent imaging using a capacitive micromachined ultrasonic transducer array. Phys Med Biol. 2014;59(17):4879-96.

17. Shanmugam P, Iglesias L, Michaud JF, Alquier D, Colin L, Dufour I, et al. Broad bandwidth air-coupled micromachined ultrasonic transducers for gas sensing. Ultrasonics. 2021;114:106410.
18. Meynier C, Teston F, Certon D. A multiscale model for array of capacitive micromachined ultrasonic transducers. J Acoust Soc Am. 2010;128(5):2549-61.
19. Merrien T, Boulmé A, Certon D. Lumped-Parameter Equivalent Circuit Modeling of CMUT Array Elements. IEEE Open Journal of Ultrasonics, Ferroelectrics, and Frequency Control. 2021;2:1-16.
20. Kamimura HA, Flament J, Valette J, Cafarelli A, Aron Badin R, Hantraye P, et al. Feedback control of microbubble cavitation for ultrasound-mediated blood-brain barrier disruption in non-human primates under magnetic resonance guidance. J Cereb Blood Flow Metab. 2019;39(7):1191-203.
21. O'Reilly MA, Hynynen K. Blood-brain barrier: real-time feedback-controlled focused ultrasound disruption by using an acoustic emissions-based controller. Radiology. 2012;263(1):96-106.
22. Chien CY, Yang Y, Gong Y, Yue Y, Chen H. Blood-Brain Barrier Opening by Individualized Closed-Loop Feedback Control of Focused Ultrasound. BME Front. 2022;2022:9867230.
23. Sun T, Zhang Y, Power C, Alexander PM, Sutton JT, Aryal M, et al. Closed-loop control of targeted ultrasound drug delivery across the blood-brain/tumor barriers in a rat glioma model. Proc Natl Acad Sci U S A. 2017;114(48):E10281-E90.
24. Tsai CH, Zhang JW, Liao YY, Liu HL. Real-time monitoring of focused ultrasound blood-brain barrier opening via subharmonic acoustic emission detection: implementation of confocal dual-frequency piezoelectric transducers. Phys Med Biol. 2016;61(7):2926-46.
25. Huang Y, Alkins R, Schwartz ML, Hynynen K. Opening the Blood-Brain Barrier with MR Imaging-guided Focused Ultrasound: Preclinical Testing on a Trans-Human Skull Porcine Model. Radiology. 2017;282(1):123-30.
26. Ji R, Karakatsani ME, Burgess M, Smith M, Murillo MF, Konofagou EE. Cavitation-modulated inflammatory response following focused ultrasound blood-brain barrier opening. J Control Release. 2021;337:458-71.
27. Cornu C, Guedra M, Bera JC, Liu HL, Chen WS, Inserra C. Ultrafast monitoring and control of subharmonic emissions of an unseeded bubble cloud during pulsed sonication. Ultrason Sonochem. 2018;42:697-703.
28. Desjouy C, Fouqueray M, Lo CW, Muleki Seya P, Lee JL, Bera JC, et al. Counterbalancing the use of ultrasound contrast agents by a cavitation-regulated system. Ultrason Sonochem. 2015;26:163-8.
29. Novell A, Escoffre JM, Bouakaz A. Second harmonic and subharmonic for non-linear wideband contrast imaging using a capacitive micromachined ultrasonic transducer array. Ultrasound Med Biol. 2013;39(8):1500-12.
30. Pouliopoulos AN, Burgess MT, Konofagou EE. Pulse inversion enhances the passive mapping of microbubble-based ultrasound therapy. Appl Phys Lett. 2018;113(4):044102.
31. Fletcher SP, Choi M, Ogrodnik N, O'Reilly MA. A Porcine Model of Transvertebral Ultrasound and Microbubble-Mediated Blood-Spinal Cord Barrier Opening. Theranostics. 2020;10(17):7758-74.
32. Zangabad RP, Lee H, Zhang X, Sait Kilinc M, Arvanitis CD, Levent Degertekin F. A High Sensitivity CMUT-Based Passive Cavitation Detector for Monitoring Microbubble Dynamics During Focused Ultrasound Interventions. IEEE Trans Ultrason Ferroelectr Freq Control. 2024;PP.